Nanoscale

Accepted Manuscript

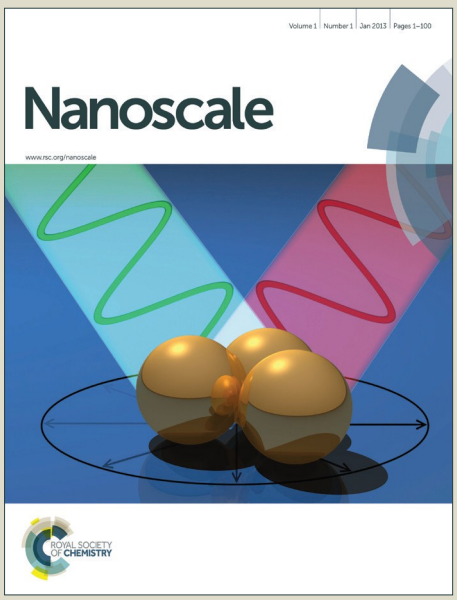

ROYAL SOCIETY OF CHEMISTRY

www.rsc.org/nanoscale

Solid state carbon nanotube device for controllable trion electroluminescent emission

Shuang Liang,[†] Ze Ma,[†] Nan Wei,[†] Huaping Liu,[ζ] Sheng Wang,[†,*] Lian-Mao Peng[†,*]

[†]Key Laboratory for the Physics and Chemistry of Nanodevices and Department of Electronics, Peking University, Beijing 100871, China

[ζ]Beijing National Laboratory for Condensed Matter Physics and Collaborative Innovation Center of Quantum Matter, Institute of Physics, Chinese Academy of Sciences, Beijing 100190, China

[*]Address correspondence to shengwang@pku.edu.cn, lmpeng@pku.edu.cn

Abstract: Semiconducting carbon nanotube (CNT) has direct chirality-dependent bandgap and reduced dimensionality-related quantum confinement effects, which are closely related to the performance of optoelectronic devices. Here taking advantages of large energy separations between neutral singlet excitons and charged excitons, i.e. trions in CNTs, we achieved for the first time all trion electroluminescence (EL) emission from chirality-sorted (8,3) and (8,4) CNTs based solid state devices. We showed that strong trion emission can be obtained as a result of localized impact excitation and electrically injected holes, with an estimated efficiency of ~5×10^{-4} photons per injected hole. The importance of contact-controlled carrier injection (including symmetric and asymmetric contact configurations) and EL spectral stability as gradually increasing bias were also investigated. The realization of electrically-induced pure trion emission opens a new opportunity for CNT film-based optoelectronic devices, providing a new degree of freedom in controlling the device to extend potential applications in spin or magnetic optoelectronics fields.

Keywords: carbon nanotube, optoelectronic device, electroluminescence, trion emission

Introduction

Because of the direct band structure, rapidly improved chirality-separation strategies and excellent nano-optoelectronic properties,[1,2] carbon nanotubes (CNTs) are being intensively investigated as active or channel materials for near infrared (IF) optoelectronics applications. Photon absorption in CNTs produces excited electrons and holes (e^--h^+) pairs, which is particularly effective under resonance excitation condition. The excited electrons and holes relax rapidly and form bound quasiparticle states, known as excitons with binding energies typically larger than a third of the bandgap energy of relevant CNTs. As a result of the strong short-range Coulomb interaction in the reduced one-dimensional (1-D) structure and consequently large binding energy, excitons usually dominate optical response of CNTs, exhibiting strong light-matter interactions that are electrically controllable, polarized dipole-like radiation and absorption, and exciton-phonon or exciton-electron scattering processes.[3] Unfortunately, even in high-quality CNTs, not all excitons can contribute to radiative recombination. Indeed among totally 16 types of excitons in a perfect CNT, only one type, i.e. singlet exciton with the odd-parity is "bright". The other 15 types of excitons are optically forbidden, and these "dark" excitons include even-parity singlet excitons and triplet excitons. In addition, quenching sites that capture potentially radiative excitons, adsorbents, metal tubes and substrates also significantly affect the efficiency of radiative recombination.[4] Nevertheless, recent researches have demonstrated that the normally optical forbidden "dark states", e.g. triplet excitons, can be lightened by introducing localized sp^3 bonds,[5,6] or designed chemical modifications.[7,8] In addition, some imperfections, exemplified by localized potential centers in CNTs, can also be considered as dimensionality modifications (e.g. zero-dimension-like dots) and hopefully provide new radiative pathways.[9,10] These discoveries further enrich intrinsic and defects-related optical properties of CNTs and provide new possibilities to artificially control luminescence processes.

Trions, charged excitons with an extra charge and nonzero spin, have been investigated extensively in conventional semiconductors and low-dimensional materials.[11] With the recent developments of chirality-sorted (high-purity) CNTs techniques, clear observations of trions in doped smaller-diameter CNTs have been made with photoluminescence (PL) or absorption spectra, and the existence of trions has been verified in both pristine and chemically doped CNTs.[12,13] Furthermore, via electrochemical doping, mixed modes of singlet exciton and trion

emissions were also observed from electrolyte-gated ambipolar devices, but pure trion emission was not realized and the electrolyte-gated device configuration is not suitable for real applications.[14] Indeed, unlike conventional heterostructures or two-dimensional (2-D) materials, the 1D configuration of CNTs provides a larger energy separations between singlet excitons and trions states (especially for smaller-diameter CNTs), via exchange energy ($\propto \sim 70/d^2$, d being the diameter of the CNT) and binding energy ($\propto \sim 60/d$, tens of meV).[15] In general, the exchange interaction lifts the energy level of the singlet state well above that of the triplet state, and the binding energy of the trion can be regarded as the energy separation between that of the triplet excitons and the trion states. The merit of such a large exciton binding strength is that it can ensure the stable existence of trions in CNTs at temperature well above room temperature and the formation of trions by other mechanisms, e.g. impact excitation dominated by unipolar carriers. Besides, it is widely believed that chemically doped CNTs are not very stable in nature, due to various electron transfer processes and the extremely environmental sensitivity. To avoid these instabilities, here we used a doping-free method to fabricate devices based on chirality-sorted CNTs. To our knowledge, this is the first report on electrical impact excitation induced trion emission from solid state CNT devices. Briefly, controllable injection of electrons or/and holes into CNTs is realized by selecting n-type (e.g. Sc) or p-type (e.g. Pd) contacts.[16] In principle, both electrons and holes, or just holes may be injected into the active channel of a CNT device, providing a highly controllable method for bright singlet exciton emission via e^--h^+ recombination, or relatively pure trion emission via impact excitation mechanism. In contrast to earlier studies on trions by optical excitation or electrolyte-gated devices, solid state devices used in this work may be readily applied for such areas as excitonic spin manipulation,[17] spin light emitting diode,[18] optical interconnect and quantum logical devices.[19] The availability of solid-state exciton (including trion) emitters also provides an ideal platform for understanding the dynamics of exciton and trion in the 1-D system,[20-22] even at high temperature. We showed that pure trions emission is obtained as a result of localized impact excitation and unipolar carriers injection. This all electrically drived trion emission opens a new radiation pathway for CNT film-based optoelectronic devices, and provides the opportunity for potential applications in multifunctional optoelectronics.

Results and Discussions

Characteristics and mechanism of EL emission

Figure 1a shows the device structure we used in this study. All devices were fabricated on silicon substrate, covered with a 100-nm-thick silver (Ag) layer, a 100-nm-thick silicon dioxide (SiO_2) layer and a 30-nm-thick hafnium oxide (HfO_2) layer. Ag layer was introduced to fully screen luminescence interference from Si substrate. In addition, a filter was used before the spectrometer to filter out background light, ensuring a reliable analysis of EL properties of CNT samples and devices. Electrodes used were 50-nm-thick palladium (Pd), with a channel length L_{ch} ~1-μm and contact width L_c ~1-μm. Atomic force microscopy (AFM) observation reveals individual CNTs with lengths between 0.7-1.3 μm and many tube-tubes junctions (Figure 1b). PL excitation (PLE) map (Figure 1c) shows that the CNT samples are dominated by (8,3) and (8,4) tubes, and the resonance excitation (λ_{ex}) and emission wavelengths (λ_e) for (8,3) CNTs are λ_{ex}= 668 nm and λ_e= 966 nm (1.283 eV); and for (8,4) CNTs λ_{ex}= 592 nm and λ_e= 1120 nm (1.1 eV).[23] While the signal associated with (7,5) CNTs is also visible in PLE, further analysis shows that the content of (7,5) CNTs is very low, giving a very weak (basically undetectable) peak in most of EL spectra. The representative PL (using a 633-nm laser) and EL spectra of the CNT films used in this work show obvious peaks in Figure 1d, which may be respectively attributed to (8,3) and (8,4) CNTs. PL and EL spectra are compared and marked by two vertical dashed lines in Figure 1d, showing obvious energy separations of ~210 meV for (8,3) CNTs and ~140 meV for (8,4) CNTs, regardless of detailed device parameters (i.e. channel length L_{ch} and source-drain bias) and fabrication processes. Here, we propose that charged exciton, i.e. trions are responsible for the observed peak shift shown in Figure 1d, and we begin our discussion and analysis by elaborating EL mechanism in CNT films.

Shown in Figures 2a and 2c are typical EL spectra of our CNT devices. Similar to III-V semiconductors, we can divide EL mechanisms in CNTs into three categories, i.e. thermal excitation, e^--h^+ recombination and impact excitation. We first rule out thermal excitation as the main mechanism responsible for the observed EL emissions. This is because large bandgaps of 1.303 eV for (8,3) tubes and 1.116 eV for (8,4) tubes are involved, which are many times larger than the thermal agitation energy k_BT at room temperature (~26meV). For e^--h^+ recombination mechanism, a large amount of electrons and holes should be simultaneously injected into the active channel of the device. This can be realized for CNT devices by utilizing asymmetric

contacts, e.g. injecting electrons using Sc electrode and injecting holes using Pd electrode. The injected electrons and holes rapidly form excitons when they encounter with each other, and some of them may decay radiatively. In this mechanism, "bright" singlet exciton emission from perfect or pristine CNTs is typically observed.[24] However, in our devices, symmetric Pd contacts were used. Since Pd contact injects mainly holes into the device channel when suitably biased, the device is basically unipolar in nature and is not suitable for e^--h^+ recombination mechanism.

While unipolar devices are not suitable for EL emission via e^--h^+ recombination mechanism, strong emission can still be achieved via impact excitation mechanism, e.g. by using a CNT crossing a narrow trench.[25] The abruptly change in the dielectric constant over the trench may lead to a strong localized electric-field and thus significantly enhanced efficiency of impact excitation. It should be noted that external factors (e.g. defect-complex or the tube-junction) in 1D systems may lead to a stronger electrostatic modification for realizing localized excitation than in three-dimensional (3-D) solids, providing naturally favorable conditions for achieving impact excitation.[25-27] Moreover, in CNTs stable trions may exist even at relatively high temperature environment, especially for smaller CNTs with d<1 nm. Figure 2a illustrates several EL spectra measured at relatively low bias, which can be fitted well by two Lorentz peaks. Quantitative analysis of the fitting shows that the integrated peak intensity has a non-linear dependence on the source-drain bias, in accordance with the impact excitation mechanism (for details, see Figure S1 in Supporting Information). The relatively large current before the threshold voltage for light emitting can be ascribed to impact excitation mechanism. For the impact excitation mechanism, EL can only be observed after the source-drain bias reaches a threshold voltage. More quantitatively, we carried out the data fitting of the emission intensity (Figure 2b) by using the impact ionization model in CNTs,[25,26]

$$\ln I \propto \frac{-E_{\mathrm{th}}}{\sqrt{\left(eF_{\mathrm{eff}}\lambda_{\mathrm{ph}}\right)^2+b^2}} \quad , \qquad (1)$$

where λ_{ph} is the optical phonon mean free path (~15 nm), and b is a thermal energy related parameter. The threshold energy E_{th} and the excitation field F_{eff} may be approximated as E_{g} and αV_{ds}, respectively. The integrated intensity shown in Figure 2b can be fitted perfectly using equation (1), with $b = 5\times10^{-2}$ (eV) and $\alpha = 4.57\times10^{-3}$ nm^{-1} for the peak associated with (8,3) CNTs and $b = 5\times10^{-2}$ (eV) and $\alpha = 3.8\times10^{-3}$ nm^{-1} for (8,4) CNTs, showing excellent agreement

with earlier reports.[25,26] Furthermore, devices with L_{ch} = 0.5, 4 and 7 μm were also fabricated and investigated with gradually increased bias, showing basically unchanged peak positions (Figure 2c and Figures S1c-d). Investigation of the L_{ch} scaling on emission properties were also carried out, showing basically a perfect linear dependence of the threshold voltage V_{Th} (the smallest voltage for observing EL emission) on L_{ch} (Figure 2d), which in turn indicates a uniformly distributed emission sites along the channel regions.

According to the impact excitation model, excitation will not occur when excitation energy is smaller than the exciton (or the trion) formation energy. We can thus estimate the density of EL emission sites (N_{es}~1-2 μm^{-1}), according to the linear relation between V_{Th} and L_{ch} shown in Figure 2d. On the other hand, it is well established that if emissions were resulted from e^--h^+ recombination, then peak energies should have been strongly affected by energy relaxation effects, leading to a shift of emission peaks and much broadened peak width in shorter channel devices.[28] Figure 2c shows that four typical devices with largely different L_{ch} (0.5-7 μm) but same L_c (1 μm) all have basically the same emission peak energies, confirming that the energy separations or peak positions observed are uncorrelated with L_{ch}. In our following discussions, we thus use typical results obtained from devices with $L_c \sim L_{ch} \sim 1$ μm.

Figure 2e shows schematic energy diagram, where the energy level of the singlet "bright" exciton is significantly higher than that of triplet "dark" excitons due to the exchange splitting effect, leading to a large energy separation between the singlet state and triplet state. Compared with singlet exciton, trion has an energy level which is well separated from singlet energy level (labeled by the Δ), and this energy difference can be divided into contributions from the exchange energy and the binding energy. The binding energy arises from the coalescence of the neutral exciton with an extra charge. The experimental results presented in Figures 1d and 2, ~210 (205-230) meV for (8,3) CNTs and ~140 (135-160) meV for (8,4) CNTs, are consistent with previous observations from trions emissions.[15] However, it should be noted that only (pure) trion emissions have been observed in our solid state devices, which are significantly different from earlier trions results from PL or electrolyte-gated devices, where singlet excitons have also be observed clearly.[13,14] The obvious trion emission can be mainly attributed to unipolar carriers induced localized impact excitation mechanism. It should be noted that in earlier PL experiments on perfect (defect-free) chirality-specific CNTs, a series of obvious trions emissions were also

observed without external doping, which was attributed to Auger recombination from exciton-exciton interaction induced doping effects in local sites.[13,29] In this work, because high-density excitons and trions can be created in local sites and the existence of abundant holes in the channel region, trion emission can be largely enhanced. While the injected holes in the CNT channel cannot give rise to "bright" singlet exciton emission via e^--h^+ recombination as in PL experiments, they can contribute to the formation of excitons in certain sites via impact excitation. These excitons can be rapidly charged by the readily available holes to form trions. Since cooled holes due to impact excitations or scatterings are very likely to make fast coalescence with just excited excitons.[22] Here the absence of singlet "bright" exciton emission may be attributed to the short life time of neutral excitons surrounded by abundant holes, which should be less than the radiative recombination lifetime of the neutral excitons, i.e. about 100ns. In most devices, the estimated efficiency of trions emissions is about the same as that of usual CNT light emitting diode, which is about ~8×10^{-5}-5×10^{-4} photons per injected hole.

The dependence of EL on contact configurations

In view of the fact that either or both types of carriers can be injected into CNTs via a controllable way or contact engineering,[16,24] we investigated the electrode effects on trion emission to clarify the influence of carrier injections. We first adopted asymmetrically contacted Pd-CNT-Ag device configuration, which is compared with that of symmetrically contacted Pd-CNT-Pd device, and the results are shown in Figure 3a. Since Ag has a low work function, the Fermi level of the Ag electrode thus aligns closer to the conduction band of the CNT,[30] providing more efficient electron injection into the conduction band of the CNT than that of holes into the conduction band of the CNT. When both electrons and holes are effectively injected into the channel region of the device, the usual "bright" singlet exciton emission will occur.[14,31] Figure 3a shows that, unlike the symmetric Pd-CNT-Pd device configuration we used in earlier section (shown in the top panel of Figure 3a), asymmetric Pd-CNT-Ag device configuration leads to a more complex device behavior, resulting in both the |bright" singlet exciton peaks via electron-hole pairs recombination (marked by gray fitting curves in the bottom panel of Figure 3a), and trions peaks as in symmetric Pd-CNT-Pd device configuration via impact excitation (marked by red fitting curves). The broadened emission peak at ~1.06 eV may be attributed to contributions

from trions in (8,3) CNTs and singlet excitons in (8,4) CNTs. Figure 3b shows the EL peaks as a function of position along the device channel (which has a channel length of 7-μm), showing hardly any dependence on the position. We thus conclude that dominating unipolar carrier injection and impact excitation mechanism are the primary causes for the dominating trion emissions observed in this work. Figure 3c depicts corresponding impact excitation and hole injection processes for the formation of radiative trions, where rapidly varying band edges or electric field may be attributed to defects or junctions along device channel. In asymmetrically contacted devices (Pd-Ag contacts), different EL mechanisms (i.e. impact excitation and e^--h^+ recombination) may have different luminescence efficiency, leading to complex EL spectrum which may be difficult to analyze quantitatively. Obvious singlet excitons emissions can be observed at relatively small bias. At large bias (e.g. > 6-7 V in a 1-μm device), however, the exponentially increased trion emission greatly conceals singlet excitons peaks.

Effects of chemical doping and ozone etching

Following the methods developed for investigating trions emission in CNTs by PL[12,32], we designed similar experiments to observe trion emission based on chirality-sorted CNTs. Here, CNTs were doped by immersing CNT films (not devices) into concentrated HNO_3 or NH_4F:HF solution, which have been used as p- or n-type dopants for showing trions emissions,[32] and the spectra obtained from optical excitation on doping films were compared with that obtained from devices by EL. Before our doping experiments, PL spectra were measured using raw CNT films, and a typical PL spectrum is shown in Figure 4a together with an EL spectrum from a device. After doping the CNT films into NH_4F:HF or HNO_3 solution, we note that new peaks appear at the same energies as that of EL emission peaks, and at the same time the original emission peaks associated with singlet excitons emissions were weakened (shown in the center panels of Figure 4a). These results agree with earlier reports on PL emission of trions, which was attributed to the introduced defects (sp^3-like metastable adducts, which can be formed on CNT-sidewalls around available active sites) and doping effect.[32] Subsequently, as a new step, we put the doped films into an ozone container for 3 min etching. The CNT films were further etched by ozone, the emission peaks associated with singlet excitons reappear (see the bottom panel of Figure 4a) and that with trions are largely suppressed, regardless of how the films were initially treated, i.e. by

HNO_3 or NH_4F:HF. Treating CNTs with ozone may lead to the following effects on the sample, which help to destruct trions: (1) neutralizing n-type dopants introduced, e.g. by NH_4F:HF; (2) removing externally introduced localized sites or states responsible for trions emissions, e.g. sp^3 defects from NO_3 or protons. We note that for other untreated samples, weak trion emission from optical excitation can be observed when the samples were exposed to air for several days (see Figure S2 in Supporting Information). This is due to the high sensitivity of CNT films to oxygen adsorption, which is known to be able to p-dope CNT and thus charge certain types of sites or defects on films, e.g. sp^3-like defects,[33,34] and convert usual neutral excitons around these sites into charged excitons. Similar case was also observed earlier,[32] where trion emission achieved by optical excitation was attributed to the diffusion of neutral excitons into defect-induced trapping sites filled by charges. Very recently, the PL research with varying gate-voltage imposed on suspended CNTs have observed trion emission, confirming the effectiveness of the electrostatic doping method.[35] Similarly, gate-voltages induced quenching effect on trions and peak shifts of ~10-15 meV are observed in present EL study. But the observation depend sensitively on local environment, especially so for CNTs on substrate.

We also treated devices with ozone to further understand electrically-induced trion emission mechanism and stability, and possible effects of etching-induced defects on emissions. Figure 4b shows that trions emissions still dominate ozone-treated devices, without observable singlet exciton emission, which is very different from that of PL observation shown in the bottom panel of Figure 4a. In PL experiment, equal numbers of electrons and holes are excited which is most suitable for neutral excitons emissions. On the other hand, in EL experiment the existence of abundant holes in the excitation regions[29] and ultrafast charged processes from excitons to trions[22] will lead to dominating trion emission as shown in Figure 4b. Figure 4c depicts normalized EL efficiency of trion emission with ozone treatment time, showing a monotonous decrease of trion emission efficiency.

EL spectral evolution with bias

Previous studies about trions in CNTs have predicted their limited temperature stability, it is thus interesting to see how EL varies as bias. To explore the voltage-dependent behavior of trion emission, an additional 20-nm-thick HfO_2 film was coated on top of the device to better avoid oxidative damage, and the temperature of the device was estimated via Raman measurements

(for details, see Figure S3).[36] Figure 5 shows some typical EL spectra which were measured when the bias was gradually increased from low (~3.5 V) to high (~ 18 V). We noted that energy positions of trions remain basically unchanged when the bias was increased, implying that trion emissions are still dominant.[37] The slight variations of the spectral profile can be attributed to the possible decomposition of trions under such a large bias (temperature) or strong electric field effect and so on.

Conclusions

In summary, controlled pure trion emission is realized using chirality-sorted CNT film based solid state device, with a symmetrical Pd-CNT-Pd configuration. It is shown that dominating trion emission results from localized impact excitation mechanism and unipolar nature of carriers in the symmetrical contact device configuration. When an asymmetrical Pd-CNT-Ag device configuration is used, both electrons and holes may be injected into the device and emission from both neutral excitons and trions are observed. Chemical and temperature stability of trion emission is also investigated. We believe that controllable emission from trions with non-zero spin could provide a new possibility for excitonic spin manipulation in CNT-film based optoelectronic devices and open a new radiation paths for optically forbidden exciton states, providing more efficient light emission.

Experimental Section

Device fabrication: The Silicon wafer was adopted as the supporting structure, covered with ~500-nm-thick thermal-oxide SiO_2. The stacking layers, i.e. $Ag/SiO_2/HfO_2$ were deposited orderly, and devices were fabricated on stacking layers to screen any signals from Si substrate. The SiO_2 and Ag layers were grown by e-beam evaporator, and HfO_2 was grown by atomic layer deposition (ALD) at 110℃. The CNTs were grown by high-pressure catalytic carbon monoxide (HiPco) decomposition, and separated by the gel chromatography method, and dispersed into 2% DOC solution. The CNTs were transferred onto HfO_2 layer by dip-coating method. For the chemical processing, the concentrated HNO_3 is ~65 wt.%, and the buffer solution NH_4F:HF is the mixture with the ratio of 7 NH_4F:1 HF. For some doping processing such as NH_4:HF, the tubes were first dropped onto the Si wafer, and were covered by 300-nm-thick PMMA600 K,

then immersed into NH_4:HF solution for three days. After etching thermal oxide layer SiO_2 in the HF acid, the exfoliated PMMA layer with CNTs was coated onto HfO_2 layer. The procedure avoids chemical reactions between Ag and HF acid. The raith150 e-beam lithography system was used to pattern devices in a ~150 nm PMMA resist. All electrical contacts, including the 50-nm-thick Pd, Ag metals, or 0.5 nm Ti/50 nm Au metals, were fabricated by e-beam evaporator through defined patterns, followed by lift-off in acetone. All device configurations are all five pairs of crossed electrodes, with L_c~1 μm and a contact crossed width of ~20 μm. The channel length L_c has a variation from 0.5 to 7 μm. In consideration of the sensitivity of CNTs to surrounding environments, devices were coated with ~150 nm copolymer layer after the fabrication. The ozone etching was carried out in model 42-220 UVO-cleaner (Jelight Company Inc.), and the modest ozone is the reaction product of the ordinary gas under UV rays. We also confirmed the same trions from CNTs devices by using other substrates, eliminating the potentially improper analysis. For the trion emission, we also excluded the spin-orbital induction effect from heavy metal electrodes or its residual particles on CNTs by using light-metal aluminum (Al) or scandium (Sc) electrodes in independent fabrications.

Raman, PL and EL measurements: All spectra measurements were carried out under the focus condition, by UV-NIR HR800 confocal microscope system, equipped with a liquid-nitrogen-cooled InGaAs detector and a CCD (charge-coupled device). For PL and EL measurements, the grating of 150 grooves/mm and a Leica microscope objective (50×, NA=0.55) were used. The light emitted from CNTs was filtered by an optical band-pass filter with the high transmission window between 800 to 1700 nm, filtering all possible excitation source (633 nm laser). For PLE spectra, the sorted HiPco samples in aqueous solution were confirmed with a spectrofluorometer (HORIBA, NanoLog) and the step of excitation or emission wavelength was 5 nm. For Raman measurements, the scattered light was separated from the excitation source by a filter, detected by spectral system with the grating of 1800 grooves/mm, having a resolution of 0.3 cm^{-1}. Before and after measurement, the spectrometer system was checked by the single-crystal Si to ensure the correctness. An ambient probe station coupled to the semiconductor characterization system (Keithley 4200) was applied for electrical measurements. All these ensured that the measurement processes were stable and repeatable.

Acknowledgements

This work was supported by the National Science Foundation of China (Grant Nos. 61370009, 61271051, 61390504, 61321001 and 1427901), and Beijing Municipal Science and Technology Commission (Grant No Z151100003315009). S.L. acknowledges support by China Postdoctoral Science Foundation (2014M550559). H.L. acknowledges support by the recruitment program of global youth experts and the "100 talents project" of CAS.

ADDITIONAL INFORMATION

The authors declare no competing financial interest.

Figures and captions

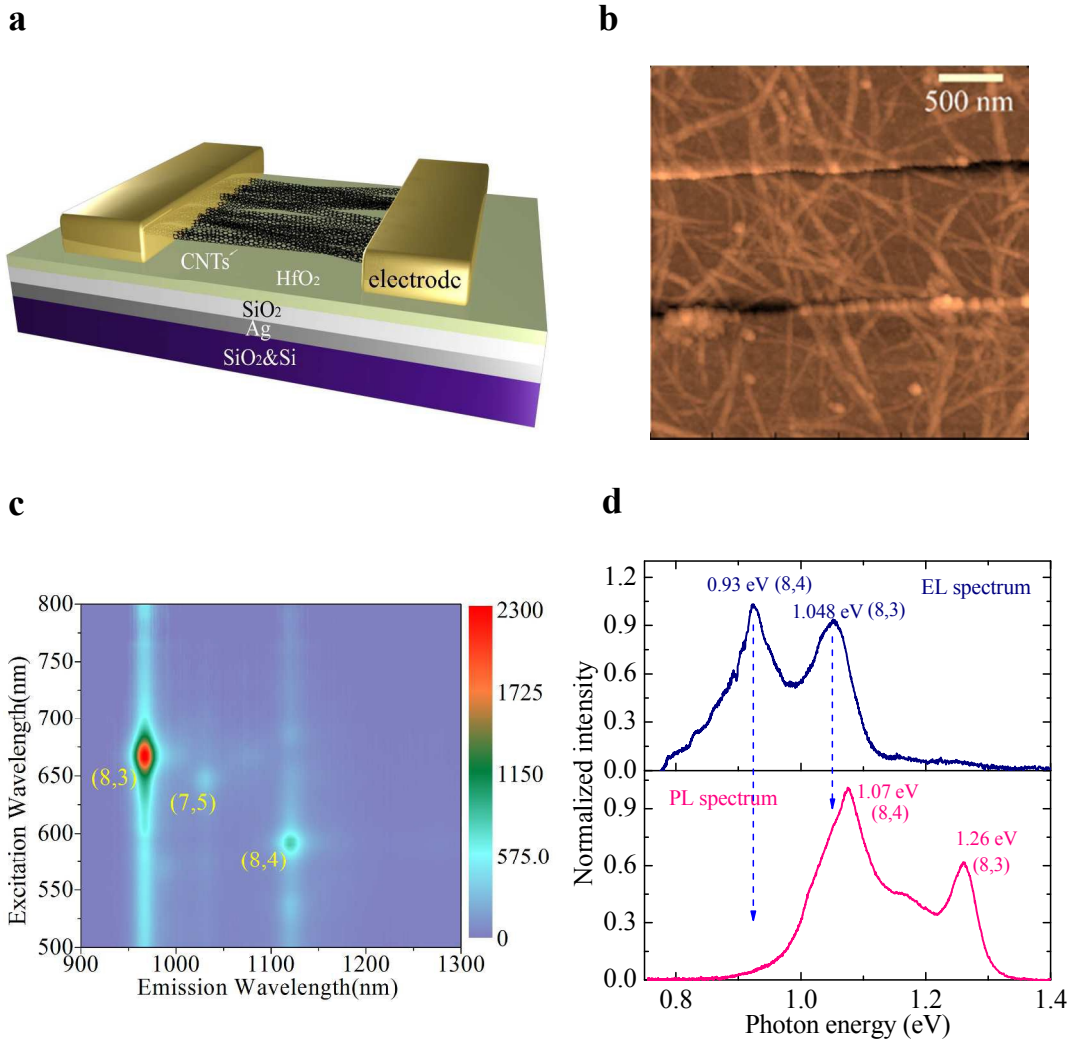

Figure 1. (a) Schematic representation of the device used in this work. The source and drain electrodes made of Pd (50 nm) or Ti/Au (0.5/50 nm) are separated by a channel with L_{ch} ~1 μm, and contact with a length L_c ~1 μm. (b) AFM image of a real device. (c) PLE map indicates the dominant chirality population from (8,3) and (8,4) tubes. (d) Comparison between EL and PL spectra, showing redshifts of ~210 meV for the peak associated with (8,3) nanotubes and ~140 meV for the peak associated with (8,4) nanotubes. The PL spectrum was obtained by optical excitation using 633-nm laser.

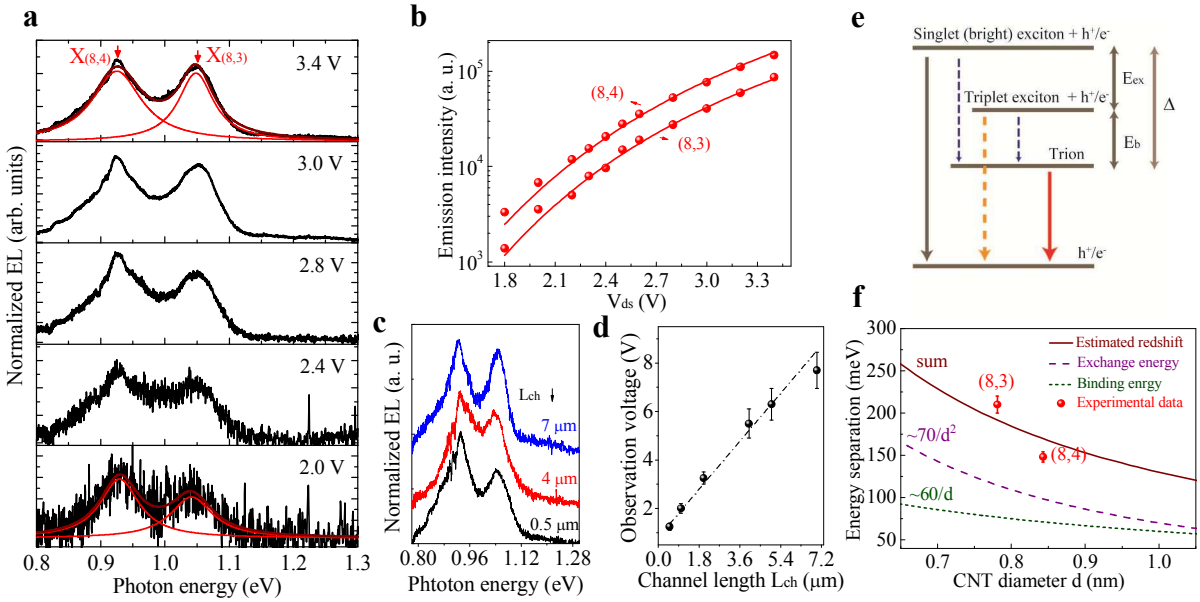

Figure 2. (a) Typical EL spectra measured at different bias, fitted by Lorenz peaks. X represents the trion peak. (b) Integrated intensities from (8,4) and (8,3) peaks versus the bias, which are fitted using impact excitation model. (c) EL spectra from devices with different L_{ch}, confirming unanimous profiles, at the bias of 1.5, 5, and 8 V for devices with L_{ch} = 0.5, 4 and 7 μm, respectively. (d) Dependence of threshold observation voltage on L_{ch}, showing basically a linear relation. (e) Schematic energy diagram and luminescence processes associated with "bright" singlet exciton (gray line), "dark" triplet exciton (orange line) and the trion (red line). (f) Energy separation (Δ) between the singlet and the trion state versus tube diameter d. Red circle: observed values in this experiment. Theoretical results are also shown, including the sum Δ, exchange energy E_{ex} ($\propto \sim 70/d^2$) and binding energy E_b ($\propto \sim 60/d$), respectively.[15]

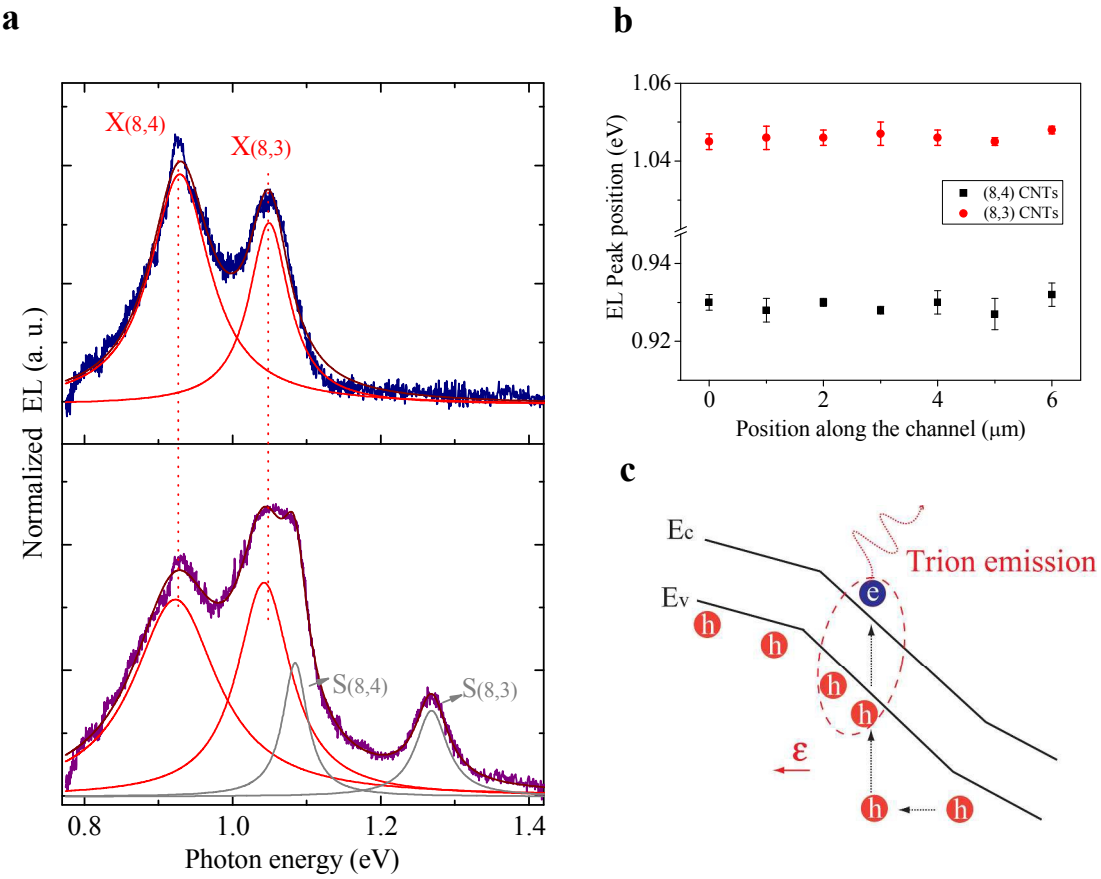

Figure 3. (a) EL spectra measured from devices with different contacts. Top panel: EL spectrum from devices with symmetric Pd electrods, measured at ~3 V. Bottom panel: EL spectrum from a device with asymmetric Pd-Ag electrodes, measured at ~4 V, showing obvious singlet exciton peaks labeled by S (8,3) and S (8,4). (b) The nearly constant peak positions of trion EL emissions, independent of the position in channel regions. (c) Schematic diagram of impact excitation and doping effect for creating the radiative trions.

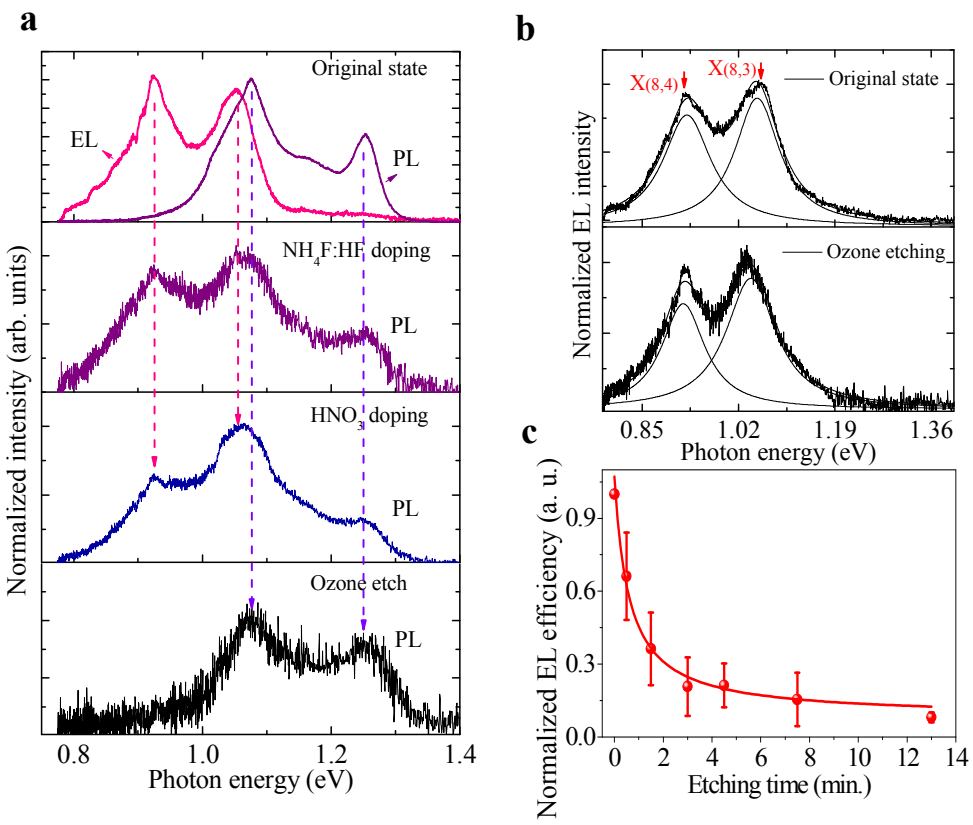

Figure 4. (a) PL spectra showing the luminescence evolution, from unintentionally doped CNTs (original state), after NH_4F:HF treatment, after HNO_3 treatment, and after ozone etching. (b) Unchanged EL spectra after ozone etching on devices. The dominance of trion emission is confirmed. (c) Normalized trion EL efficiency as a function of etching time, showing reduced trion emission with increasing etching time. The entire process of optical excitation was investigated with the 633-nm laser.

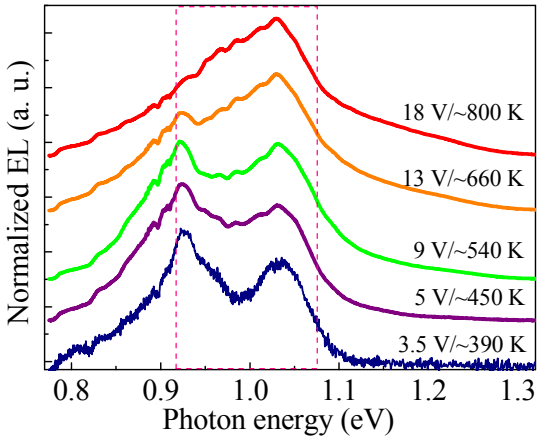

Figure 5. Normalized EL spectra measured at gradually increased bias (temperature).

Notes and references

1 H. P. Liu, D. Nishide, T. Tanaka and H Kataura, *Nature Commun.*, 2011, **2**, 309.

2 Avouris, P.; M. Freitag and V. Perebeinos, *Nat. Photonics.*, 2008, **2**, 341.

3 J. A. Misewich, R. Martel, P. Avouris, J. C. Tsang, S. Heinze and J. Tersoff, *Science*, 2003, **300**, 783.

4 D. M. Harrah and A. K. Swan, *ACS Nano*, 2011, **5**, 647.

5 Y. M. Piao, B. Meany, L. R. Powell, N. Valley, H. Kwon, G. C. Schatz and Y. H. Wang, *Nat. Chem.*, 2013, **5**, 840.

6 A. H. Castro Neto and F. Guinea, *Phys. Rev. Lett.*, 2009, **103**, 026804.

7 H. Harutyunyan, T. Gokus, A. A. Green, M. C. Hersam, M. Allegrini and A. Hartschuh, *Nano Lett.*, 2009, **9**, 2010.

8 A. D. Mohite, T. S. Santos, J. S. Moodera and B. W. Alphenaar, *Nat. Nanotech.*, 2009, **4**, 425.

9 Y. Miyauchi, M. Iwamura, S. Mouri, T. Kawazoe, M. Ohtsu and K. Matsuda, *Nat. Photonics,* 2013, **7**, 715.

10 S. Ghosh, S. M. Bachilo, R. A. Simonette, K. M. Beckingham and R. B. Weisman, *Science*, 2010, **330**, 1656.

11 K. F. Mak, K. L. He, C. Lee, G. H. Lee, J. Hone, T. F. Heinz and J. Shan, *Nat. Mater.*, 2013, **12**, 207.

12 R. Matsunaga, K. Matsuda and Y. Kanemitsu, *Phys. Rev. Lett.*, 2011, **106**, 037404.

13 S. M. Santos, B. Yuma, S. Berciaud, J. Shaver, M. Gallart, P. Gilliot, L. Cognet and B. Lounis, *Phys. Rev.*

Lett., 2011, **107**, 187401.

14 F. Jakubka, S. B. Grimm, Y. Zakharko, F. Gannott and J. Zaumseil, *ACS Nano*, 2014, **8**, 8477.

15 Y. Kanemitsu, *Phys. Chem. Chem. Phys.,* 2011, **13**, 14879.

16 L. M. Peng, Z. Y. Zhang, S. Wang and X. L. Liang, *AIP Adv.*, 2012, **2**, 041403.

17 C. Galland and A. Imamoglu, *Phys. Rev. Lett.*, 2008, **101**, 157404.

18 J. P. Wang, A. Chepelianskii, G. Feng and N. C. Greenham, *Nat. Commun.*, 2012, **3**, 1191.

19 S. Khasminskaya, F. Pyatkov, B. S. Flavel, W. H. Pernice and R. Krupke, *Adv. Mater.*, 2014, **26**, 3465.

20 S. Mouri, Y. Miyauchi, M. Iwamura and K. Matsuda, *Phys. Rev. B*, 2013, **87**, 045408.

21 N. Akizuki, M. Iwamura, S. Mouri, Y. Miyauchi, T. Kawasaki, H. Watanabe, T. Suemoto, K. Watanabe, K. Asano and K. Matsuda, *Phys. Rev. B*, 2014, **89**, 195432.

22 T. Koyama, S. Shimizu, Y. Miyata, H. Shinohara and A. Nakamura, *Phys. Rev. B*, 2013, **87**, 165430.

23 R. B. Weisman and S. M. Bachilo, *Nano Lett.*, 2003, **3**, 1235.

24 S. Wang, Q. S. Zeng, L. J. Yang, Z. Y. Zhang, Z. X. Wang, T. Pei, L. Ding, X. L. Liang, M. Gao, Y. Li and L. M. Peng, *Nano Lett.*, 2011, **11**, 23.

25 J. Chen, V. Perebeinos, M. Freitag, J. Tsang, Q. Fu, J. Liu and P. Avouris, *Science*, 2005, **310**, 1171.

26 N. Hibino, S. Suzuki, H. Wakahara, Y. Kobayashi, T. Sato and H. Maki, *ACS Nano*, 2011, **5**, 1215.

27 M. Freitag, J. C. Tsang, J. Kirtley, A. Carlsen, J. Chen, A. Troeman, H. Hilgenkamp and P. Avouris, *Nano Lett.*, 2006, **6**, 1425.

28 M. Freitag, V. Perebeinos, J. Chen, A. Stein, J. C. Tsang, J. A. Misewich, R. Martel and P. Avouris, *Nano Lett.*, 2004, **4**, 1063.

29 B. Yuma, S. Berciaud, J. Besbas, J. Shaver, S. Santos, S. Ghosh, R. B. Weisman, L. Cognet, M. Gallart, M. Ziegler, B. Hönerlage, B. Lounis and P. Gilliot, *Phys. Rev. B* 2013, **87**, 205412.

30 H. B. Michaelson, *J. Appl. Phys.*, 1977, **48**, 4729.

31 J. S. Ross, P. Klement, A. M. Jones, N. J. Ghimire, J. Q. Yan, D. G. Mandrus, T. Taniguchi, K. Watanabe, K. Kitamura, W. Yao, D. H. Cobden and X. D. Xu, *Nat. Nanotech.*, 2014, **9**, 268.

32 A. H. Brozena, J. D. Leeds, Y. Zhang, J. T. Fourkas and Y. H. Wang, *ACS Nano*, 2014, **8**, 4239.

33 H. Hiura, T. W. Ebbesen, J. Fujita, K. Tanigaki and T. Takada, *Nature*, 1994, **367**, 148.

34 P. G. Collins, K. Bradley, M. Ishigami and A. Zettl, *Science*, 2000, **287**, 1801.

35 M. Yoshida, A. Popert and Y. K. Kato, *Phys. Rev. B* 2016, **93**, 041402.

36 H. D. Li, K. T. Yue, Z. L. Lian, Y. Zhan, L. X. Zhou, S. L. Zhang, Z. J. Shi, Z. N. Gu, B. B. Liu, R. S. Yang, H. B. Yang, G. T. Zou, Y. Zhang and S. Iijima, *Appl. Phys. Lett.*, 2000, **76**, 2053.

37 I. V. Bondarev, *Phys. Rev. B*, 2014, **90**, 245430.